SEISMIC EFFECTS OF VISCOUS BIOT-COUPLING: FINITE DIFFERENCE SIMULATIONS ON MICRO-SCALE

E.H. Saenger, S.A. Shapiro, and Y. Keehm

email: *saenger@geophysik.fu-berlin.de*
keywords: *finite-difference modeling, viscous fluids, Biot theory*

ABSTRACT

This paper is concerned with numerical considerations of viscous fluid effects on wave propagation in porous media. We apply a displacement-stress rotated staggered finite-difference (FD) grid technique to solve the elastodynamic wave equation. An accurate approximation of a Newtonian fluid is implemented in this technique by using a generalized Maxwell body. With this approach we consider the velocity predictions of the Biot theory for elastic waves in different digital rock samples. To distinguish between the low and the high frequency range we estimate the effective permeabilities by a flow simulation. Our numerical results indicate that the viscous Biot-coupling is visible in the numerical experiments. Moreover, the influences of other solid-fluid interactions (e.g. Squirt flow) are also discussed.

INTRODUCTION

Although the theory of seismic wave propagation in porous fluid-saturated media has been established 50 years ago (Biot, 1956) there are still many unanswered questions about the origin of attenuation and dispersion in such media. In particular, while it is generally accepted that these dissipative effects can be explained by the presence of wave-induced flow phenomena, there is still no consensus on the mathematical model of these phenomena. Some of the questions about the physics of wave propagation in porous materials can be addressed by numerical simulations performed on the micro-scale, that is, on the scale of individual pores and grains. Having this in mind, Saenger et al. (2004b) already have performed such wave propagation simulations based on the rotated staggered grid (RSG) finite-difference (FD) technique (Saenger et al., 2000). However, they have restricted themselves to determine effective elastic properties of porous media saturated with a non-viscous fluid.

In this paper we extend this approach to a Newtonian (i.e. viscous) fluid. We propose an accurate approximation of a viscous fluid saturating a porous solid using a generalized Maxwell body. This is a well-known rheological model, which has been previously used to simulate (nearly) constant frequency-independent attenuation by a time-domain FD scheme (Emmerich and Korn, 1987; Kristek and Moczo, 2003).

In a second part of this paper, we use the proposed method to test the applicability of the Biot velocity relations (Biot, 1956) to porous materials. We explicitely simulate elastic waves in porous solid structures saturated with a viscous fluid. This means that our modeling involves all solid-fluid interactions which are covered by the elastodynamic wave equation. The goal here is to identify explicitely the seismic effect of the viscous Biot-coupling in the numerical experiments.

The flow simulations additionally performed in this paper are carried out for the determination of the reference frequency of the Biot theory. These simulations provide a combined estimate of transport and mechanical properties of the same digital rock sample.

DIGITAL ROCK SAMPLES

To generate realistic synthetic microstructures we use an approach described in Roberts and Garboczi (2002), the so-called open-cell Gaussian random field (GRF) scheme. The porespace is defined by the intersection of two two-cutted Gaussian random fields (i.e. Gaussian A and Gaussian B; see Table 1 for details). To ensure a complete connectivity of the pores we eliminate isolated pores. In this paper we use exact the same GRF's as in Saenger et al. (2004b). Figure 1 shows one typical realization (GRF3).

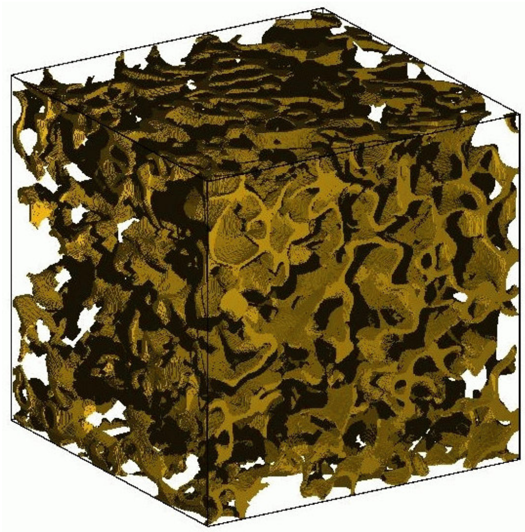

Figure 1: An open-cell Gaussian random field (GRF3). The structure shown is the porespace, the transparent part is the grain material.

Permeability values were estimated through the Lattice-Boltzmann (LB) flow simulations on the synthetic digital rocks. The biggest advantages of the LB method are that it is readily applied to any arbitrary discrete geometry (Keehm et al., 2004) and that it describes fluid flow in porous media very accurately (Ladd, 1994; Keehm, 2003). We used the time-averaged velocity scheme (Ladd, 1994) to avoid artifacts in local velocity fields. The numerical flow simulation was performed with an assigned pressure gradient (∇P) across opposite faces of cubical digital rocks. We imposed no-flow boundary condition on the other four side faces of the cube. From the simulated local flux field, we calculated a volume-averaged flux $< q >$. Then, the macroscopic permeability (κ) was estimated using the Darcy's law:

$$< q >= \frac{\kappa}{\eta} \nabla P \tag{1}$$

where η is the dynamic viscosity of the fluid. We repeated the LB simulation with 1-D pressure gradient for all three directions and the permeability was estimated by averaging three permeability values (κ_x, κ_y and κ_z). We did not observe any significant anisotropy of permeability in the synthetic digital rocks. With the permeability (Table 1) it is possible to calculate the Biot reference frequency (Table 2).

VISCOELASTIC WAVE SIMULATIONS

Theoretical model of viscoelasticity

We reformulate the approach described by Emmerich and Korn (1987) and Kristek and Moczo (2003). Incorporation of viscosity based on the generalized Maxwell body (GMB) means that Hooke's law is modified:

$$\sigma_{ij} = c_{ijkl}\epsilon_{kl} - \sum_{m=1}^{n} \xi_m^{ij}. \tag{2}$$

MEDIUM	GRF 1	GRF 2	GRF 3	GRF 4	GRF 5
Porosity ϕ	3.42%	8.77%	13.2%	8.02%	21.6%
Perm. κ $[10^{-4}(\Delta x)^2]$	9.780	151.5	500.6	33.1	647.6
Gaussian A					
corrl. len. $[0.0002m]$	25	25	25	13	25
cut min.	0.4	0.4	0.4	0.4	0.38
cut max.	0.6	0.6	0.6	0.6	0.62
Gaussian B					
corrl. len. $[0.0002m]$	30	30	30	15	14
cut min.	0.485	0.48	0.4575	0.4904	0.46
cut max.	0.515	0.52	0.5415	0.5296	0.54

Table 1: Details of the open-cell GRF models (size: 400^3 gridpoints, $\Delta x = 0.0002m$). Every single model (GRF1-5) is build up of the intersection of two two-level cutted Gaussian random fields (Gaussian A and B).

In this equation, $\sigma_{ij},\ c_{ijkl},\ \epsilon_{kl}$ denote the stresses, the elastic tensor and the strains, respectively. The number of relaxation mechanisms is equal to n. The anelastic functions ξ_m^{ij} are determined by:

$$\dot{\xi}_m^{ij} + \omega_m \xi_m^{ij} = \omega_m \tilde{Y}_m^{ijkl} \epsilon_{kl}, \tag{3}$$

with $\tilde{Y}_m^{ijkl}$ as the tensors of anelastic coefficients and ω_m as angular relaxation frequencies. The GMB frequency-dependent viscoelastic modulus $C_{ijkl}(\omega)$ can be derived by inserting the Fourier transform of equation (3) into equation (2):

$$C_{ijkl}(\omega) = c_{ijkl} - \sum_{m=1}^{n} \tilde{Y}_m^{ijkl} \frac{\omega_m}{i\omega + \omega_m}. \tag{4}$$

Using this formalism it is possible to implement attenuation in a general anisotropic media.

Implementation of viscoelasticity in a displacement-stress rotated staggered grid scheme

A second-order discretization in time of equation (3) yields (compare with discretization of equation (28) of Emmerich and Korn (1987)):

$$\xi_m^{ij}(t + 1/2\Delta t) = \frac{2 - \omega_m \Delta t}{2 + \omega_m \Delta t}\ \xi_m^{ij}(t - 1/2\Delta t) + \frac{2\omega_m \Delta t}{2 + \omega_m \Delta t}\ \tilde{Y}_m^{ijkl} \epsilon_{kl}(t). \tag{5}$$

This can be implemented in a displacement-stress finite difference algorithm as shown in Moczo et al. (2001). They point out that this is the most efficient FD scheme for incorporating attenuation models. One main feature of the RSG is that all components of one physical property are placed in an elementary cell at one single location. This is also true for the anelastic functions ξ_m^{ij} and the tensor of anelastic coefficients $\tilde{Y}_m^{ijkl}$. These parameters are located at the same position as the stiffness tensor (see Fig. 1(d) of Saenger et al. (2000)).

Approximation of a Newtonian fluid using a generalized Maxwell body

A compressible viscous fluid is charcterized by the following frequency-dependent elastic moduli (Auld, 1973):

$$C_{44}(\omega) = \mu(\omega) = i\omega\eta_\mu, \tag{6}$$

$$C_{12}(\omega) = \lambda(\omega) = \lambda(0) + i\omega\eta_\lambda, \tag{7}$$

with $\lambda(\omega)$ and $\mu(\omega)$ as angular-frequency dependent Lamé parameters. For all examples in this paper we assume that $\eta_\mu = \eta_\lambda = \eta$. The key problem is how to approximate the viscous behaviour given by equation (6) and (7) using a GMB. The following strategy (illustrated in Figure 2) is based on a Taylor-expansion of equation (4) around $\omega = 0$:

- We use one relaxation mechanism (n=1).

- $\tilde{Y}_1^{44} = c_{44}$. Only in this case it is possible that $C_{44}(0) = 0$ [compare with equation (6) and (4)].

- In the low frequency range of the GMB, using one relaxation mechanism, the wanted fluid-viscosity can be determined by the following relations:

$$\eta_\mu = \frac{1}{i} \left. \frac{\partial C_{44}(\omega, \tilde{Y}_1^{44} = c_{44})}{\partial \omega} \right|_{\omega=0} = \frac{c_{44}}{\omega_1}, \tag{8}$$

$$\eta_\lambda = \frac{1}{i} \left. \frac{\partial C_{12}(\omega)}{\partial \omega} \right|_{\omega=0} = \frac{\tilde{Y}_1^{12}}{\omega_1}. \tag{9}$$

- From $\eta_\mu = \eta_\lambda$ it follows $\tilde{Y}_1^{12} = c_{44}$. Further, with equation (4), (7) and the known relation $c_{11} = c_{12} + 2c_{44}$ we obtain:

$$c_{11} = \lambda(0) + 3c_{44}. \tag{10}$$

- For FD approaches it is necessary to take into account the stability criterion. For the rotated staggered grid with FD operators of second order in time and space the following relation is valid (Saenger et al., 2000):

$$\sqrt{\frac{c_{11}}{\rho_{fluid}}} = v_p \leq \gamma, \quad \gamma = \frac{\Delta h}{\Delta t}. \tag{11}$$

- We choose c_{44} from the following range [given by the 'stability criterion'-relation (11) and equation (10)]:

$$c_{44} \leq \frac{\gamma^2 \rho_{fluid} - \lambda(0)}{3}. \tag{12}$$

  Together with the choice of the angular relaxation frequency ω_1 one can determine the wanted dynamic viscosity η [compare with equation (8)].

- We choose a source signal in the low frequency range of the applied GMB ($2\pi f_{source} << \omega_1$).

Wave propagation modeling procedure

We apply the 3D RSG-technique with the viscoelastic extension described above to explicitely model wave propagation in fluid saturated porous media. The synthetic porous rock-models are embedded in a homogeneous elastic region. The full models are made up of 804x400x400 grid points with an interval of Δx=0.0002m. In the homogeneous region and for the grain material we set a P-wave velocity of v_p=5100m/s, a S-wave velocity of v_s=2944m/s and a density of ρ_{grain}=2540kg/m^3. For dry pores we set v_p=0m/s, v_s=0m/s and ρ_v=0.0001kg/m^3. For the fluid-filled pores we use the parameters given in Table 2. We perform our modeling experiments with periodic boundary conditions in the two horizontal directions. To obtain effective velocities in different models we apply a body force plane source at the top of the model. The plane P- or S-wave generated in this way propagates through the porous medium. We measure the time-delay of the peak amplitude of the mean plane wave caused by the inhomogeneous region. Using the time-delay we estimate the effective velocity and, therefore, also the corresponding elastic moduli (see Table 2). The source wavelet is the first derivative of a Gaussian with a dominant frequency of $f_{source} = 8 \times 10^4 Hz$ and with a time increment of $\Delta t = 2.1 * 10^{-8} s$. All computations are performed with second order spatial FD operators and with a second order time update. A similar numerical setup with a detailed error analysis is discussed in Saenger et al. (2004a).

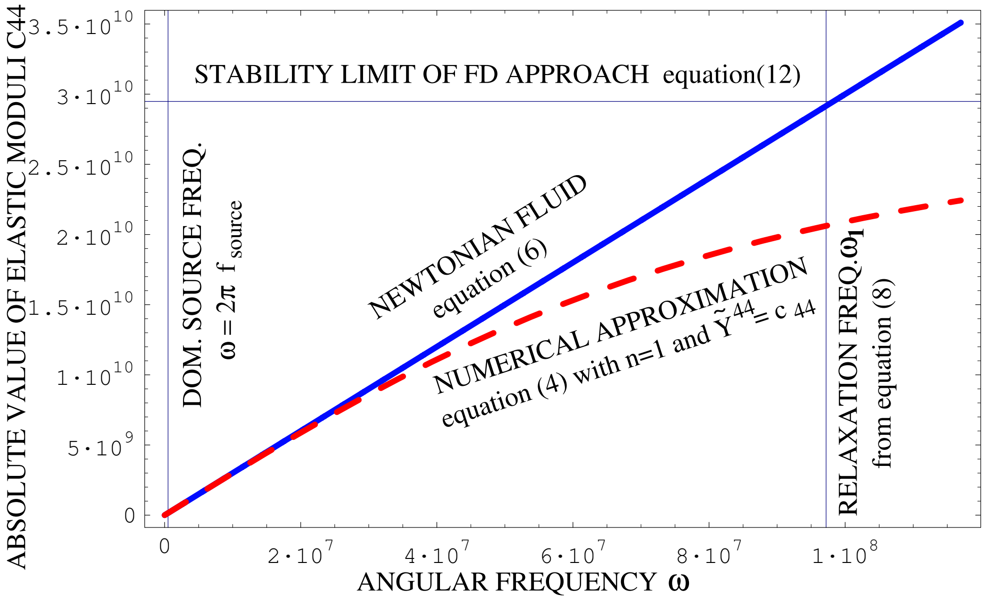

Figure 2: Absolute values of the shear modulus C_{44} in dependence of the angular frequency ω. In the frequency range of the used source the precision of the numerical approximation of the Newtonian fluid is very high. Parameters are taken from experiment 13 (Table 2).

INTERPRETATION OF NUMERICAL RESULTS

Permeability versus static dry elastic moduli

Experiments No. 1,2,3,9 and 15 (see Table 2) provide the effective dry rock moduli of the digital rock samples GRF 1-5. As expected we observe an increasing permeability with an increasing porosity (Table 1). Also elastic moduli decrease with increasing porosity. We make the following observations: First, the permeability varies over two orders of magnitude whereas the effective elastic moduli varies about 30%. Second, the permeability varies with the poresize (i.e. Δx) whereas the static elastic moduli are scale independent.

Viscous versus non-viscous pore fluid

In experiments No. 4,5,10 and 11 (Table 2) we consider effective elastic moduli of GRF3 and GRF4 saturated with a non-viscous and a Newtonian fluid of normal density ($\rho_{fluid} = 1000kg/m^3$). However, the theoretical differences of the low- and the high-frequency limit of Biot are in these cases not significant enough to clarify unambiguously if the Biot effect is visible in the synthetics (exact formulae can be found e.g. in Mavko et al. (1998)). This change significantly if we use a fluid with an artificially high density ($\rho_{fluid} = 15000kg/m^3$):

- Using a non-viscous high-density fluid for pore saturation [experiment 6,12 and 16 of Table (2)] we consider the high frequency limit of Biot (: viscosity $\eta = 0$; hence, the reference frequency f_{biot} can be determined for our rock-models with a non-zero permeability κ using $f_{biot} = \phi\eta/(2\pi\rho_{fluid}\kappa)$ as zero; see e.g. Mavko et al. (1998)). This enables us to estimate the corresponding tortuosity of the rock models [see Figure (3) and Saenger et al. (2004b) for details].

- Using a high-density Newtonian fluid with a viscosity of $\eta = 1000kg/(ms)$ for pore saturation [experiment 7,13, and 17 of Table (2)] we consider the low frequency limit of Biot because the dominant frequency of the propagating wave [$f_{source} = 8\times10^4Hz$] is clear below the Biot reference frequency. We observe a reduction of the effective elastic moduli towards the theoretical predicted

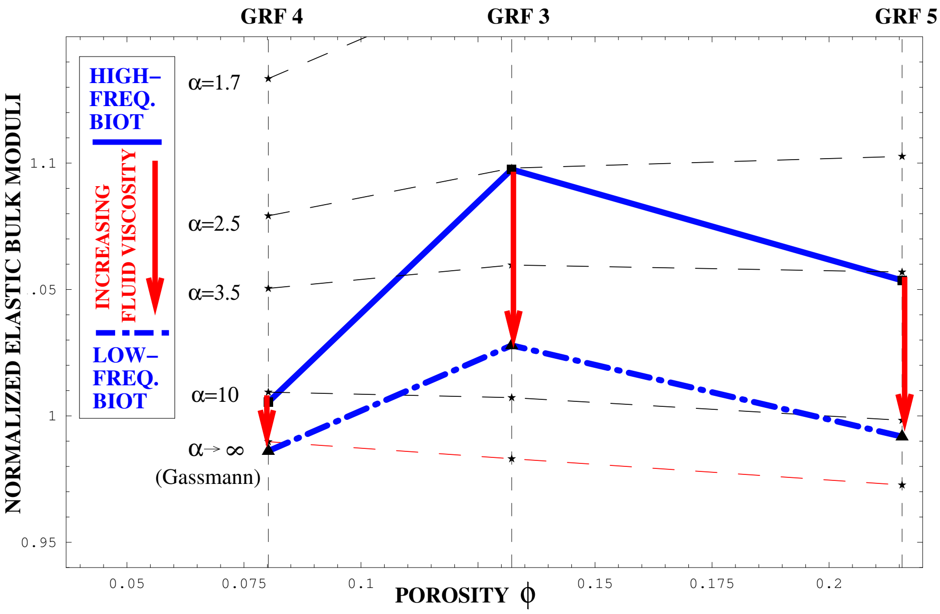

Figure 3: The normalized effective bulk modulus ($< K > /K_{grain}$) versus porosity for GRF 3,4 and 5 saturated with a non-viscous (thick solid line) and a Newtonian [$\eta = 1000kg/(ms)$; dash-dotted thick line] fluid of artificially high density ($\rho_{fluid} = 15000kg/m^3$). The dashed lines display the high frequency limit of the Biot theory calculated from $< K_{dry} >$ using different values for the tortuosity α.

low-frequency limit of Biot (i.e. Gassmann; derived from the dry case) in comparison to experiment 6,12 and 16. This is shown in Figure 3 for the effective bulk modulus.

The interpretation of this result is as follows: The seismic effect of the Biot theory is clearly visible in our numerical wave propagation experiments.

However, we have fixed three physical reasons why we still observe some numerical deviations from Biot's predictions (i.e. for GRF 3 and 5 the observed low-frequency value is not consistent with Gassmann; see Figure 3):

- The unknown influence of Squirt. The critical frequency of this flow as well as the amount of soft porosity is very difficult to estimate for our used models (for details see Mavko et al. (1998)).
- The relatively high velocity of shear waves (most significant for experiment 8 and 14) in the fluid ($v_s = \sqrt{|i\omega\eta_{fluid}/\rho_{fluid}|}$) is not included in Biot and Squirt theories; this effect can be roughly estimated by analysing the upper Hashin-Sthrikmann bound (e.g. Mavko et al. (1998)) using $\mu_{fluid} = v_s^2\rho_{fluid}$ and $\omega = \omega_{source}$ (see Table 2).
- Local anisotropy in overall isotropic heterogeneous porous media (for details see Berryman (2004))

CONCLUSIONS

In this paper we perform finite-difference simulations on micro-scale to study the effect of viscous Biot-coupling on wave propagation. We implement a generalized Maxwell body (Emmerich and Korn, 1987; Kristek and Moczo, 2003) into a displacement-stress rotated staggered grid scheme with the result that all viscous parameters are located in the centre of an elementary cell. Using this technique it is possible to saturate synthetic rock models with realistic approximations of Newtonian fluids. This allows us to study all coupling mechanism of fluid-solid interaction which are covered by the elastodynamic wave equation. To estimate the reference frequency for the Biot approach we also determine the permeabilities of our digital rock samples by flow simulations. This gives us the possibility to compare mechanical and transport properties derived for exact the same digital rock samples. The wave propagation experiments in those

Table 2: Normalized effective moduli ($\hat{\mu} =< \mu > /\mu_{grain}$, $\hat{K} =< K > /K_{grain}$) for the digital rock models GRF1-5 saturated with different types of fluids. The fluid can be characterized by it elastic moduli c_{44}, the fluid viscosity η_{fluid}, the density ρ_{fluid} and the P-wave velocity at zero frequency $v_p(\omega = 0)$. Additionally we give the Biot reference frequency f_{biot} and a viscosity dependent upper Hashin-Sthrikman-bound μ_{viHS}

No.	$c_{44} of fluid$ $[10^9 kg/(ms^2)]$	$v_p(\omega = 0)$ [m/s]	ρ_{fluid} $[kg/m^3]$	η $[kg/(ms)]$	f_{biot} $[10^4 Hz]$	norm. eff. moduli	"viscosity-dependent" upper HS-bounds
				GRF 1 ($\phi = 3.42\%$)			
1	0	0	0.0001	0	- (dry)	$\hat{\mu} = 0.849$, $\hat{K} = 0.790$	$\mu_{viHS} = 0.935$
				GRF 2 ($\phi = 8.77\%$)			
2	0	0	0.0001	0	- (dry)	$\hat{\mu} = 0.605$, $\hat{K} = 0.493$	$\mu_{viHS} = 0.841$
				GRF 3 ($\phi = 13.2\%$)			
3	0	0	0.0001	0	- (dry)	$\hat{\mu} = 0.472$, $\hat{K} = 0.369$	$\mu_{viHS} = 0.770$
4	0	1485	1000	0	0	$\hat{\mu} = 0.509$, $\hat{K} = 0.529$	
5	29.16	1485	1000	300	314	$\hat{\mu} = 0.532$, $\hat{K} = 0.544$	$\mu_{viHS} = 0.773$
6	0	1485	15000	0	0	$\hat{\mu} = 0.652$, $\hat{K} = 1.097$	
7	6.694	1485	15000	1000	69.9	$\hat{\mu} = 0.602$, $\hat{K} = 1.028$	$\mu_{viHS} = 0.779$
8	6.694	1485	15000	10000	699	$\hat{\mu} = 0.735$	$\mu_{viHS} = 0.847$
				GRF 4 ($\phi = 8.02\%$)			
9	0	0	0.0001	0	- (dry)	$\hat{\mu} = 0.754$, $\hat{K} = 0.695$	$\mu_{viHS} = 0.854$
10	0	1485	1000	0	0	$\hat{\mu} = 0.759$, $\hat{K} = 0.757$	
11	29.16	1485	1000	300	2892	$\hat{\mu} = 0.764$, $\hat{K} = 0.763$	$\mu_{viHS} = 0.856$
12	0	1485	15000	0	0	$\hat{\mu} = 0.776$, $\hat{K} = 1.005$	
13	6.694	1485	15000	1000	643	$\hat{\mu} = 0.770$, $\hat{K} = 0.986$	$\mu_{viHS} = 0.860$
14	6.694	1485	15000	10000	6427	$\hat{\mu} = 0.851$	$\mu_{viHS} = 0.900$
				GRF 5 ($\phi = 21.6\%$)			
15	0	0	0.0001	0	- (dry)	$\hat{\mu} = 0.344$, $\hat{K} = 0.272$	$\mu_{viHS} = 0.650$
16	0	1485	15000	0	0	$\hat{\mu} = 0.410$, $\hat{K} = 1.058$	
17	437.4	1485	15000	1000	88.4	$\hat{\mu} = 0.440$, $\hat{K} = 0.992$	$\mu_{viHS} = 0.662$

highly heterogeneous media saturated with viscous fluids indicate that the velocity estimations of the Biot theory are visible in our numerical results.

ACKNOWLEDGEMENTS

We thank J.E. Saiers, Y. Guéguen and B. Gurevich for very useful comments and suggestions which helped to improve the paper.

REFERENCES

Auld, B. A. (1973). *Acoustic Fields and Waves in Solids, Vol. 1*. John Wiley and Sons, New York.

Berryman, J. G. (2004). Poroelastic shear modulus dependence on pore-fluid properties arising in a model of thin isotropic layers. *Geophys. J. Int.*, 157:415–425.

Biot, M. A. (1956). Theory of propagation of elastic waves in a fluid-saturated porous solid. I. Low frequency range and II. Higher-frequency range. *J. Acoust. Soc. Amer.*, 28:168–191.

Emmerich, H. and Korn, M. (1987). Incorporation of attenuation into time-domain computations of seismic wave fields. *Geophysics*, 52:1252–1264.

Keehm, Y. (2003). *Computational Rock Physics: Transport Properties in Porous Media and Applications*. PhD thesis, Stanford University.

Keehm, Y., Mukerji, T., and Nur, A. (2004). Permeability prediction from thin sections: 3D reconstruction and lattice-boltzmann flow simulation. *Geophys. Res. Lett.*, 31:L04606.

Kristek, J. and Moczo, P. (2003). Seismic-wave propagation in viscoelastic media with material discontinuities: A 3D fourth-order staggered-grid finite-difference modeling. *Bull., Seis Soc. Am.*, 93(5):2273–2280.

Ladd, A. J. C. (1994). Numerical simulations of particulate suspensions via a discretized boltzmann equation: Part 2. numerical results. *J. Fluid Mech.*, 271:311–339.

Mavko, G., Mukerji, T., and Dvorkin, J. (1998). *The Rock Physics Handbook*. Cambridge University Press, Cambridge.

Moczo, P., Kristek, J., and Bystrický, E. (2001). Efficiency and optimization of the 3-D finite-difference modeling of seismic ground motion. *Journal of Computational Acoustics*, 9(2):593–609.

Roberts, A. P. and Garboczi, E. J. (2002). Computation of the linear elastic properties of random porous materials with a wide variety of microstructure. *Proc. R. Soc. Lond. A*, 458:1033–1054.

Saenger, E. H., Gold, N., and Shapiro, S. A. (2000). Modeling the propagation of elastic waves using a modified finite-difference grid. *Wave Motion*, 31(1):77–92.

Saenger, E. H., Krüger, O. S., and Shapiro, S. A. (2004a). Effective elastic properties of randomly fractured soils: 3D numerical experiments. *Geophys. Prosp.*, 52(3):183–195.

Saenger, E. H., Krüger, O. S., and Shapiro, S. A. (2004b). Numerical considerations of fluid effects on wave propagation: Influence of the tortuosity. *Geophys. Res. Lett.*, 31:L21613.